In-Plane Microstructure of Gas Diffusion Layers With Different Properties for PEFC

Mehdi Mortazavi
Multiscale Transport Process Laboratory,
Mechanical Engineering-Engineering Mechanics,
Michigan Technological University,
Houghton, MI 49931
e-mail: mortazav@mtu.edu

Kazuya Tajiri [1]
Mechanical Engineering-Engineering Mechanics,
Michigan Technological University,
Houghton, MI 49931
e-mail: ktajiri@mtu.edu

The gas diffusion layer (GDL) is undoubtedly one of the most complicated components used in a polymer electrolyte fuel cell (PEFC) in terms of liquid and gas transport phenomena. An appropriate fuel cell design seeks a fundamental study of this tortuous porous component. Currently, porosity and gas permeability have been known as some of the key parameters affecting liquid and gas transport through the GDL. Although these are dominant parameters defining mass transport through porous layers, there are still many other factors affecting the transport phenomena and overall cell performance. In this work, the microstructural properties of Toray carbon papers with different thicknesses and for polytetrafluoroethylene (PTFE) treated and untreated cases have been studied based on scanning electron microscopy (SEM) image analysis. The water droplet contact angle, as a dominant macroscale property, along with the mean pore diameter, pore diameter distribution, and pore roundness distribution, as important microscale properties, have been studied. It was observed that the mean pore diameter of Toray carbon paper does not change with its thickness and PTFE content. Mean pore diameter for Toray carbon papers was calculated to be around 26μm, regardless of their thicknesses and PTFE content. It was also observed that the droplet contact angle on the GDL surface does not vary with the GDL thickness. The average contact angle for the 10 wt. % PTFE treated GDLs of different thicknesses was measured at about 150 deg. Finally, the heterogeneous in-plane PTFE distribution on the GDL surface was observed to have no effect on the mean pore diameter of GDLs. [DOI: 10.1115/1.4025930]

Introduction

Although the polymer electrolyte fuel cell (PEFC) has received a great amount of consideration as a clean type of energy system, there are still some technical challenges that need to be solved before this type of energy system can be commercially released. Among these challenges, one can refer to water management in the PEFC. During the operation of a PEFC, oxygen is reduced in the cathode and is accompanied by water production. Some amount of this produced water may fill the open pores of the gas diffusion layer (GDL). The GDL is a macroporous layer with multifunction purposes such as providing a uniform transport of reactants to the catalyst layer, removing excess water from the membrane by providing pathways of water to the gas channel, mechanically protecting the membrane as a fragile thin layer, and providing electrical conductivity between the electrodes and the current collectors. An appropriate design of the GDL has been reported to have a significant contribution on proper water balance within the cell [1–4].

For a continuous transport of reactants to the catalyst layer and transport of excess water to the gas channel, the GDL pores should be free from accumulated liquid water. Excess water accumulated within the GDL pores and gas flow channels blocks the flow of reactants to the catalyst layer and, finally, results in oxidant starvation and performance loss. Liquid water accumulated within the GDL pores emerges from the GDL surface in the form of droplets.

The liquid water transport mechanism on the GDL surface is a function of the superficial gas velocity, which is defined as the bulk velocity of gas flowing within the channel cross sectional area and the droplet emergence rate [5]. While for high superficial gas velocities the drag force from the shear gas flow can easily detach a water droplet from the GDL surface, a moderate or low superficial gas velocity is not capable of detaching the droplet directly from the GDL surface. Instead, the droplet grows in size until it touches the gas channel walls and spreads over them. In such cases, capillary flow drains liquid water through the corners, forming an annular film flow. For a high liquid water production rate and/or low superficial gas velocity, the water film will not be drained properly and the channel will be clogged as the liquid film grows.

Water transport mechanisms within the GDL are quite different from liquid water transport on the GDL surface and can be categorized into diffusion, pressure driven hydraulic permeation, and evaporation [6]. The liquid water behavior on the GDL surface can be studied by simple optical visualization techniques [5,7–10] while the water behavior within the GDL cannot be easily monitored. Some of the techniques used for studying the water behavior within the GDL are X-ray and neutron radiography [11] since both the X-ray and neutron beams are capable of penetrating through the GDL. However, each of these techniques has their own drawbacks. For instance, the expensive hardware of neutron imaging requires a challenging calibration to ensure a reliable data acquisition [12].

It is a common practice to treat GDLs with some hydrophobic media such as polytetrafluoroethylene (PTFE) to enhance gas transport and liquid water transport through the pores when the cell is operating at flooding condition [13]. Park et al. [14] tested GDLs with different amounts of PTFE and obtained the *I-V* curves of a single cell working at different levels of relative humidities. They concluded that among different water transport mechanisms within the GDL, evaporation and shear force are more dominant than capillary force and attributed that to the relatively large pore diameters of GDLs compared to the microporous and catalyst layers. Pasaogullari and Wang [15] used a one-dimensional analytical solution and concluded that liquid water transport within the GDL is controlled by capillary forces arising from the gradient in phase saturation. Nam and Kaviany [16] studied water transport within the GDL by developing a capillary pressure model and

[1]Address all correspondence to this author.

Contributed by the Advanced Energy Systems Division of ASME for publication in the Journal of Fuel Cell Science and Technology. Manuscript received July 29, 2013; final manuscript received September 27, 2013; published online December 4, 2013. Editor: Nigel M. Sammes.

Table 1 Properties of GDLs used in this study

Toray carbon paper type	Manufacturer specified GDL thickness (μm)	GDL thickness measured (μm)	Manufacturer specified porosity (%)	Bulk density (gcm^{-3})	Fiber diameter (μm)	Air permeability (m^2)	Areal mass ($mg\ cm^{-2}$)	PTFE concentration in emulsion (wt. %)
TGP-030	110	103	80	—	—	—	4.7	10.4
TGP-060	190	179	76 (78 [19,20])	0.44 [19]	—	—	8.6	10.3
TGP-090	280	282	78 (80 [21])	0.45 [19]	9.2 [21]	8.9×10^{-12} [21]	12.6	10.5
TGP-120	370	336	78	0.45 [19]	—	8.7×10^{-12} [8]	16.5	10.4

hypothesized that water is distributed as an "upside-down tree" capillary network. Litster et al. [17] followed a fluorescence microscopy technique and visualized liquid water transport in the GDL. They suggested that water transport within the GDL is mostly dominated by fingering and channeling in such a way that as a breakthrough path within the GDL forms, liquid water existing in other paths recedes back and finds its way through the newly formed breakthrough path. The illustrated literature review herein highlights the different and sometimes opposite hypotheses made regarding liquid water transport through the GDL.

Water transport through and on the surface of the GDL can be characterized by two independent parameters of the GDL microstructure and pore surface wettability [3]. The GDL pore diameter, for instance, was known to directly affect the water vapor pressure at which condensation occurs, according to the Kelvin equation [18], and for vapor pressures below saturation pressure, water vapor starts condensing in a pore smaller than the critical pore diameter [1]. In this article, the GDL microstructure has been studied by processing SEM images taken from untreated and treated GDLs with different thicknesses. The SEM images of Toray carbon papers with different thicknesses have been analyzed to obtain the microstructural properties such as the mean pore diameter, pore diameter distribution, and pore roundness. Since all of the GDLs used in this study have the same production procedure, we expect to obtain a similar microstructure for all of the samples used. Air permeability, on the contrary, is a property that can be used for comparing the microstructure of porous materials [19]. The very close air permeability of the GDL samples used in this

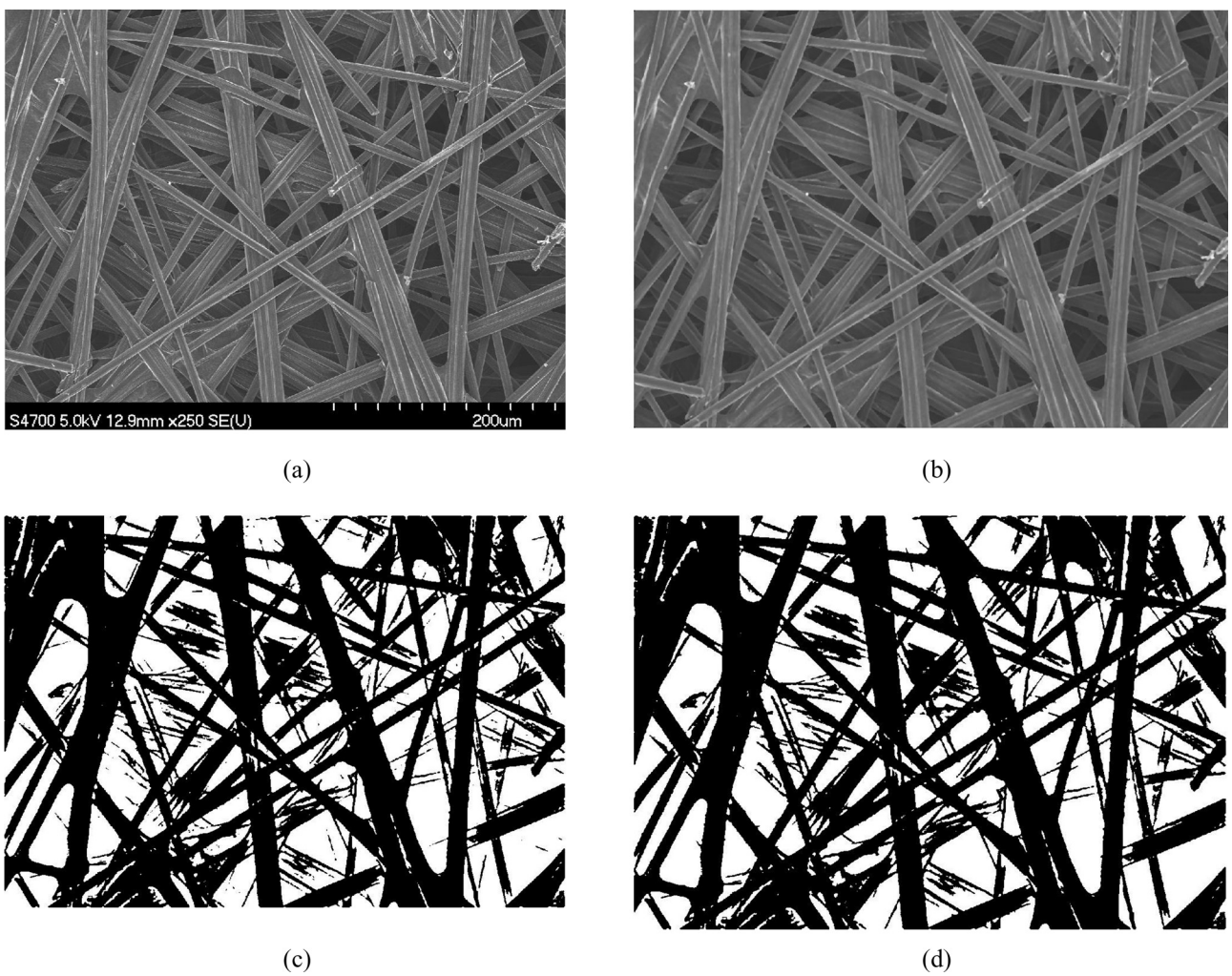

Fig. 1 SEM image processing steps

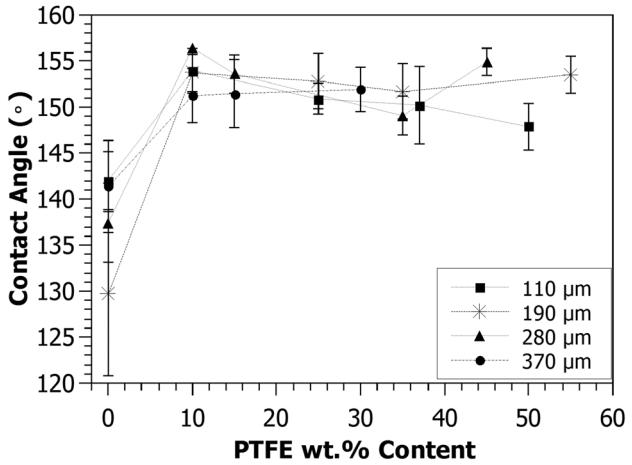

Fig. 2 Droplet contact angle on treated and untreated GDLs

study, as listed in Table 1, can be an indication of the similar microstructures of Toray carbon papers of different thicknesses [19].

Experimental

Toray carbon papers with different thicknesses were used as the GDL in this study. The GDLs with manufacturer specified thicknesses of 110 μm, 190 μm, 280 μm, and 370 μm have been used. For each thickness, untreated and 10 wt. % PTFE treated papers were tested for microstructural analysis. For the PTFE treating of the GDL samples, Toray carbon papers were loaded with PTFE based on the procedure given in Ref. [22]. This procedure is described as follows. The substrates were first dipped in the PTFE emulsion (60 wt. % dispersion in H_2O, Aldrich) for 10 h and then they were put in a furnace at 120 °C for 1 h to dry them. In order to make a uniform distribution of the PTFE within the GDL substrates, they were sintered at 360 °C for 1 h. The static contact angles of the liquid water droplets on the GDL samples with different PTFE contents were measured using a homemade setup designed and made specifically for this purpose [23] with the procedures and theory given in Ref. [24]. Ten droplets with diameters within the range of 1 − 3 mm were dropped on the GDL surfaces and the mean contact angles were considered. Table 1 lists the measured and calculated physical properties of the samples used in this study. The GDL thicknesses were measured using an electronic micrometer (Mitsutoyo, Japan). The measured thicknesses were slightly different from the thicknesses specified by the manufacturer. However, the manufacturer-specified thicknesses are used for the remainder of the paper.

The surface morphology of the GDL samples were scanned using a JEOL JSM-6400LV scanning electron microscope (SEM) at 20 keV and 250× magnification. For each sample, three random locations were chosen and images were obtained. The SEM images were analyzed for the mean pore diameter, pore diameter distribution, and pore roundness distribution based on the procedure introduced in Ref. [25]. A MATLAB code was used for analyzing the SEM raw images, first applying median filtering [26] to smoothen out the high frequency noise. The filtered images were then segmented and processed [27] by thresholding, based on the Otsu method [28] in order to convert the gray level images into binary black and white images. Thus, all of the carbon fibers became black and the empty pores of the GDL became white. Finally, the black and white images were gap-filled to remove small gaps in the fibers and the pores. In order to make the gap-filling step more accurate, pore diameters of less than 5 μm were filtered out in our analysis. Figure 1 shows the four steps of the image processing used in this study.

Results and Discussion

The SEM images were processed for microstructural analysis. The analysis includes the mean pore diameter, pore diameter distribution, and pore roundness distribution for the different GDL samples used. Other than conducting a case by case comparison for GDLs of different thicknesses and for treated and untreated sample, the pore diameter distribution for one untreated GDL sample (TGP_120) and at three different locations was also obtained, as will be discussed in the In-Plane Pore Distribution section. These distribution plots may be used to define the order of anisotropicity of GDLs in future studies but no quantitative analyses were done on them in this study. Finally, as mentioned in the Experimental section, the SEM images were processed based on the Otsu method for threshold setting. In order to examine the validity of the results obtained based on this approach, the effect of threshold setting on the mean pore diameter was also studied. Before all of these microstructural analyses, the liquid water droplet contact angles on the GDLs were measured. The contact angle is a macroscale property that represents the wetting ability of a solid surface by a liquid. It is a function of the interfacial energy along the three phase boundary. The measured contact angles can help illuminate the variation of the GDL surface energy for different PTFE contents within the GDL.

Contact Angle. The droplet contact angle describes the solid surface interfacial tensions based on Young's mechanical equilibrium relation. The liquid droplet contact angle on a solid surface such as the GDL introduces the mechanical equilibrium of the droplet under the influence of three phase interfacial tensions [29]. Furthermore, the droplet contact angle on the GDL surface is one of the most important parameters in water management with applications in the PEFC since it directly affects some major properties with dominant effects on liquid water transport within and upon the GDL surface. The surface adhesion force (given in Eq. (1)), drag force from shear gas flow in the gas channel (given in Eq. (2)), the capillary pressure, and even the droplet shape on the GDL surface are some properties that the contact angle directly affects. The surface adhesion force keeps the droplet on the GDL surface

$$F_s = 2\sigma_{lv} d_d \sin^2\theta \sin(\Delta\theta) \tag{1}$$

where σ_{lv} is the surface tension between the liquid and vapor, d_d is the diameter of a droplet upon detachment, θ is the contact

Table 2 Contact angle measured for GDLs with different thicknesses

GDL type	GDL thickness (μm)	Contact angle (deg) (untreated GDL)	Contact angle (deg) (PTFE content level no. 1)	Contact angle (deg) (PTFE content level no. 2)	Contact angle (deg) (PTFE content level no. 3)	Contact angle (deg) (PTFE content level no. 4)
TGP-030	110	142.0 ± 3.1	153.9 ± 2.4 (10 wt. %)	150.9 ± 1.7 (25 wt. %)	150.2 ± 4.3 (37 wt. %)	147.8 ± 2.5 (50 wt. %)
TGP-060	190	129.7 ± 8.8	153.7 ± 2 (10 wt. %)	152.8 ± 3 (25 wt. %)	151.7 ± 3 (35 wt. %)	153.5 ± 2 (55 wt. %)
TGP-090	280	137.4 ± 4.3	156.4 ± 1.5 (10 wt. %)	153.6 ± 2 (15 wt. %)	149 ± 2 (35 wt. %)	154.9 ± 1.5 (45 wt. %)
TGP-120	370	141.3 ± 5.0	151.2 ± 2.9 (10 wt. %)	151.4 ± 3.7 (15 wt. %)	151.9 ± 2.4 (30 wt. %)	NA

Table 3 Mean pore diameter of GDLs with different thicknesses

Toray carbon paper type	GDL thickness (μm)	Untreated GDL mean pore diameter (μm)	10 wt. % treated GDL mean pore diameter (μm)
TGP-030	110	25.23 ± 0.47	25.46 ± 0.86
TGP-060	190	25.95 ± 0.66	26.94 ± 2.27
TGP-090	280	27.68 ± 1.05	26.49 ± 3
TGP-120	370	25.45 ± 0.22	NA

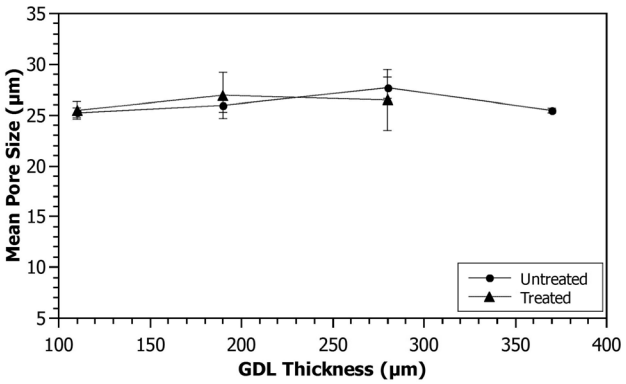

Fig. 3 GDL mean pore size as a function of its thickness

angle, and $\Delta\theta$ is the difference between the advancing and receding contact angles [5]. The drag force tries to detach the droplet from the GDL surface

$$F_D = \frac{1}{2}\rho C_D A_P V^2 \tag{2}$$

where ρ is the density of the gas flowing in the gas channel, C_D is the drag coefficient, A_P is the droplet projected area perpendicular to the gas flow, and V is the superficial gas velocity.

The static contact angles measured in this study for each GDL sample are shown in Fig. 2. The error bars represent the standard deviation calculated for each contact angle data point. It can be observed that the droplet contact angle significantly changes from an untreated to a treated GDL surface, while adding larger amounts of PTFE does not make any change on the contact angle. Furthermore, it seems that the GDL thickness does not affect the droplet contact angle. As Whitesides and Laibinis [30] reported, the droplet behavior on the GDL surface is mostly controlled by the wetting characteristics of the top few monolayers of the surface. That is why the thickness of the GDL shows no contribution to the droplet contact angle. Table 2 lists the mean contact angle measured for ten droplets being dropped on the GDLs and the calculated standard deviation. For each GDL thickness, the droplet contact angles on the untreated GDL and treated GDLs with different amounts of PTFE are shown. It can be concluded from Table 2 and Fig. 2 that the average contact angle that the droplets make is about 150 deg on treated GDLs, regardless of the PTFE content and, as mentioned earlier, the GDL thickness has no effect on this contact angle. Similar contact angles on GDLs with different PTFE contents have been observed and reported by other

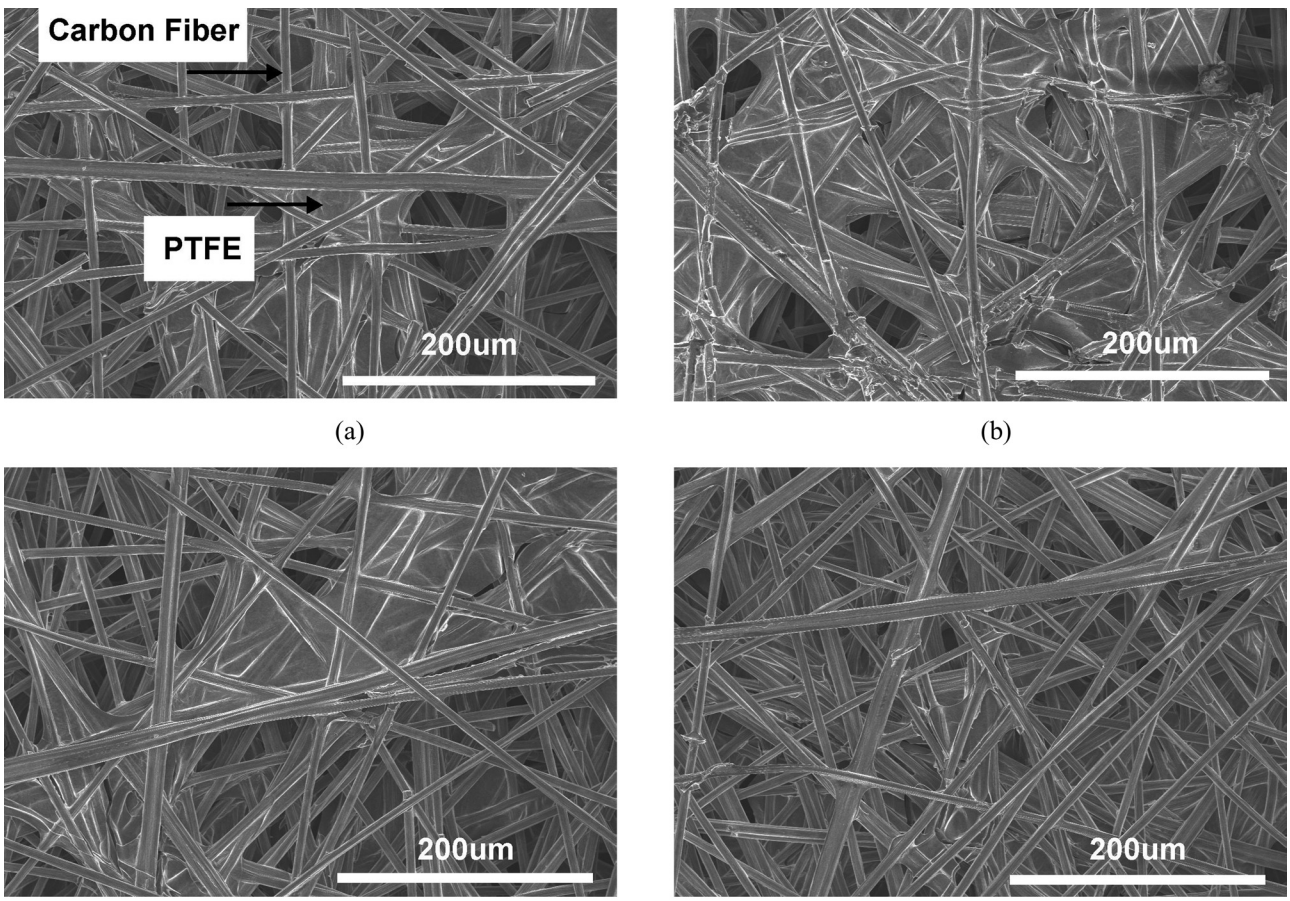

Fig. 4 SEM image of different locations on a treated GDL sample

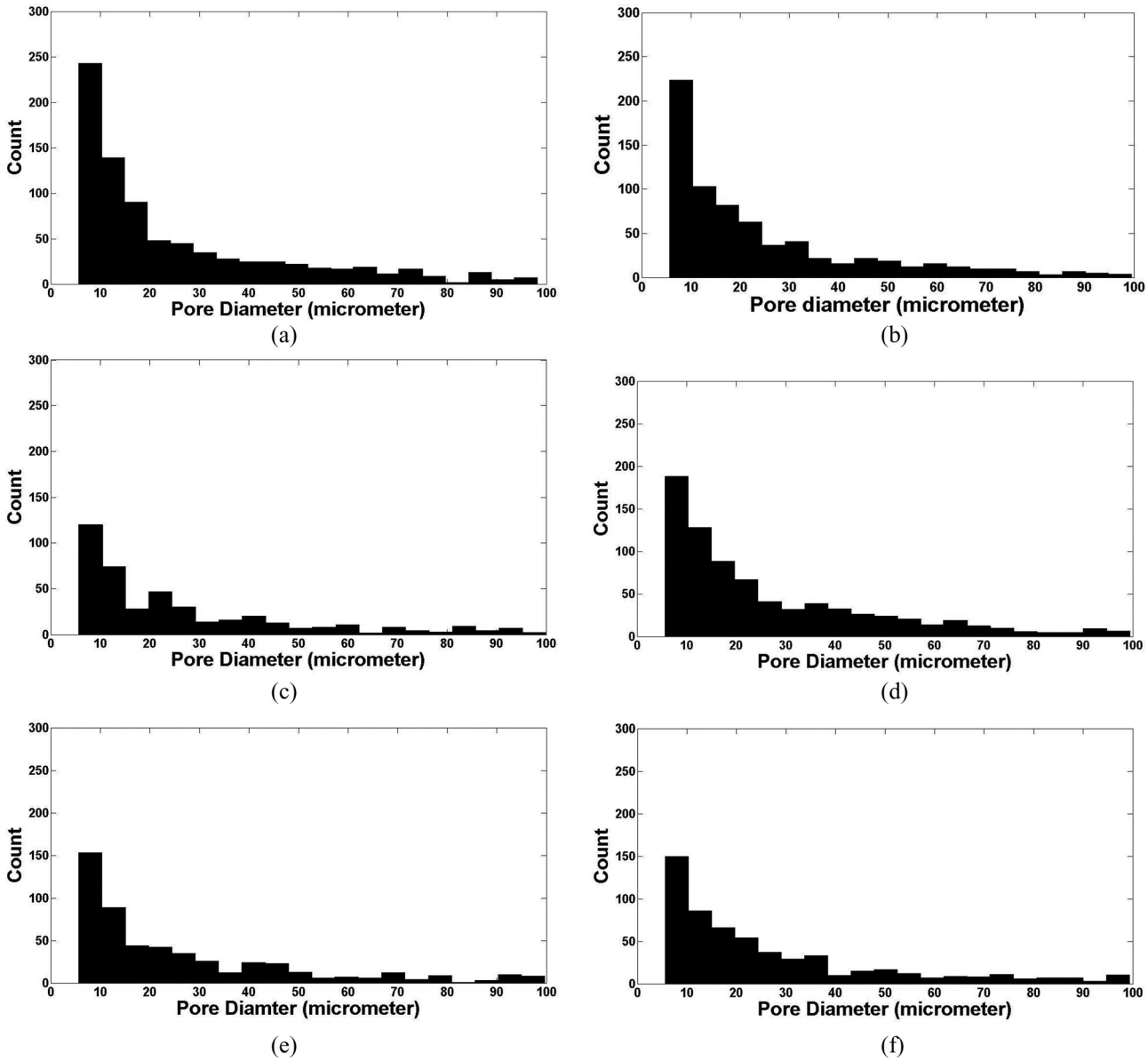

Fig. 5 Pore diameter distribution for GDLs of different thicknesses

groups such as Fairweather et al. [31] and Benziger et al. [32]. It also lead us to draw the conclusion that PTFE particles mostly penetrate through the GDL and agglomerate within the GDL, rather than sitting on its surface.

Mean Pore Diameter. The GDLs' mean pore diameters were obtained by analyzing the SEM images based on the procedure introduced by Parikh et al. [25]. For each GDL case, five SEM images were obtained with a scan size of 507 μm $\times$ 356 μm, as defined by the ImageJ software developed by the National Institutes of Health. The overall mean pore diameter was calculated by averaging the mean pore diameters obtained for each SEM image. The GDL pore diameter is characterized by the *equivalent pore diameter* (EPD), given by Eq. (3)

$$\text{EPD} = 2\sqrt{A/\pi} \tag{3}$$

where A is the area of the pore [33].

The GDL pore size is one of the most important parameters in liquid water transport from the catalyst layer, where water is produced as one of the byproducts of the electrochemical reaction, to the gas channel, where it can be drained, either by detachment caused by shear gas flow or corner flow across the edges of the gas channels [5]. Liquid water passes through the GDL pores when its pressure exceeds the capillary pressure and, for a continuous flow, its pressure should remain higher than the capillary pressure [16]. Capillary pressure is defined as the difference between the pressure of the liquid and gas phase at equilibrium ($P_c = P_l - P_g$) and is a function of the mean curvature of the water-air interface, contact angle, and surface energy

$$P_c = \frac{2\sigma_{\text{water}} \cos\theta}{r_{\text{pore}}} \tag{4}$$

where σ_{water} is the interfacial surface tension, θ is the contact angle, and r_{pore} is the pore radius. The smaller the pore radius, the greater the capillary pressure liquid water should overcome to be able to pass through the GDL. Tamayol and Bahrami [19] modeled the GDL as a network of pores connected by throats. Based on their model, it is assumed that air and liquid water are stored in the pores and the volume occupied by the throats is negligible.

Only throats resist liquid water transport and pores do not have any resistance to the flow [34]. It was reported that the capillary pressure increases with the Toray carbon paper thickness [19]. Based on the model discussed in Ref. [19], as the thickness of the GDL increases, the number of layers forming the GDL also increases. This directly increases the breakthrough pressure of the liquid water. Table 3 lists the mean pore diameter calculated for GDLs of different thicknesses. Based on the results obtained by this approach, the GDL mean pore diameter is not changing with the GDL thickness and even the mean pore diameters for untreated and treated GDLs are the same. The mean pore diameter obtained for all GDLs is about 26 μm, which is in good agreement with the mean pore diameter reported by Parikh et al. [25] for Toray carbon paper. The mean pore size given in Refs. [8,35] is within the range of $30-40$ μm, that is, again, in agreement with the results obtained in this work.

Considering the average pore diameter of 26 μm, average contact angle of 150 deg, and water surface tension of 0.072 Nm^{-1}, the capillary pressure will be calculated at 9.5 kPa, based on Eq. (4). This pressure is almost twice as much as the breakthrough pressure reported in Ref. [36]. The reason behind this is that for a mean pore diameter of 26 μm, there are some pores with larger diameters in the GDLs that result in lower capillary pressure and, as Bazylak et al. [37] had reported, liquid water chooses the path of least resistance through the GDL and emerges from the surface of the GDL in the form of droplets. A further discussion about pore diameter distribution will be given in the Pore Diameter Distribution section. Figure 3 shows the calculated mean pore diameter as a function of the GDL thickness both for treated and untreated GDLs. As mentioned earlier, the mean pore diameter does not change, neither with the GDL thickness nor with the PTFE content, within the GDL. The PTFE particles are within the range of $50-500$ nm [38], which is much smaller than the mean pore diameter.

Figure 3 and Table 3 also show a higher standard deviation of the mean pore diameter for treated GDLs compared to untreated ones. The SEM images of the treated GDL surface are shown in Fig. 4. As shown in Fig. 4, the white areas between the carbon fibers are the PTFE emulsion dried on the surface of the GDL. Figure 4 shows that, even for the same GDL, the sample PTFE is not uniformly distributed and there can be some areas with higher PTFE content (see Fig. 4(*b*)) and some areas with lower PTFE content (see Fig. 4(*d*)). Other than the uneven PTFE distribution in the plane of the GDL, Fig. 4 shows that the PTFE emulsion mostly covers the top layers of the GDL and it seems from the figure that the PTFE hardly penetrates into the GDL. The same observation has been reported by Lim and Wang [39] when they took SEM images of carbon papers treated with fluorinated ethylene propylene. However, this observation is in discrepancy with the conclusion drawn from the contact angle measurement. The PTFE distribution through the GDL will be studied further by the authors. Rofaiel et al. [38] had measured the heterogeneous through-plane PTFE distribution in carbon papers by using SEM energy dispersive X-ray spectrometry and detected a larger concentration of fluorine (as the PTFE's high concentration element) along the surface fibers and less fluorine in the central region of the GDL. Fishman and Bazylak [40] measured the through-plane porosity distribution of GDLs and concluded that the PTFE accumulates at a local minima near the surface of the paper GDLs. The SEM images taken for this study, however, cannot be used for the PTFE through-plane distribution analysis.

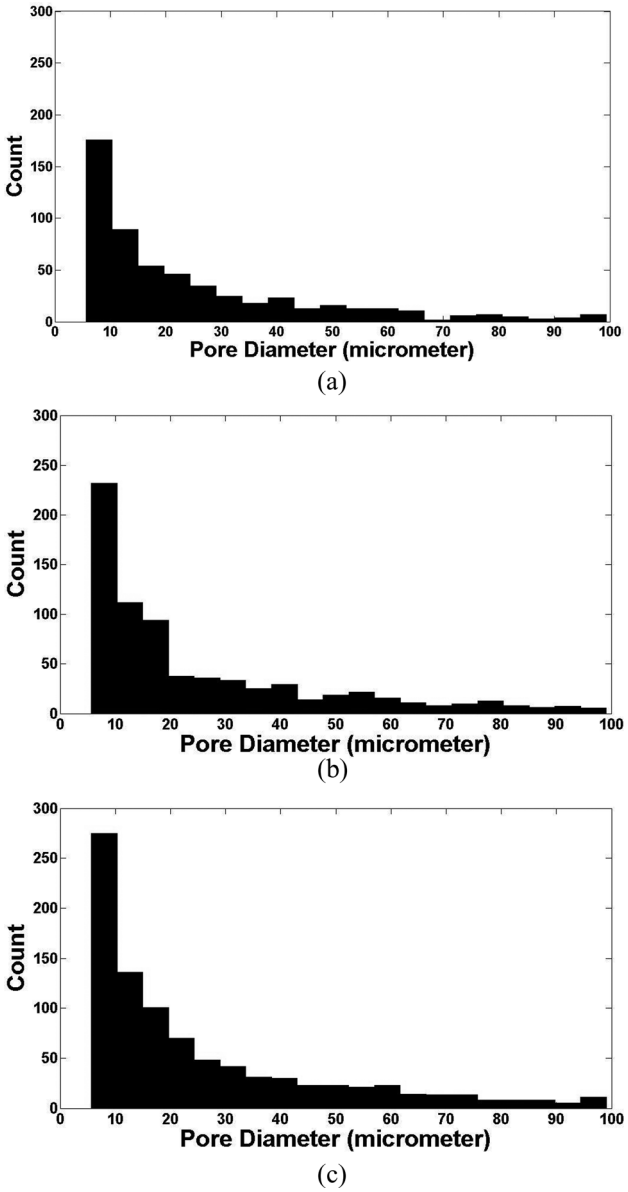

Fig. 6 Pore diameter distribution for three random locations on untreated TGP-120

Pore Diameter Distribution. Pore diameter distributions were obtained from the MATLAB code and are shown in Fig. 5 for each GDL sample. It can be concluded that for both treated and untreated GDLs, the majority of pores have diameters of less than 20 μm. However, the existence of larger pores mitigatesthe liquid water transport through the GDL by lowering the capillary pressure required for intrusion. Furthermore, pore diameter distributions show that the thinnest GDL (TGP_030) has more pores compared to the other two GDLs. This can be interpreted as the thinnest GDL is more porous compared to other samples. This result is in good agreement with the manufacturer specified porosity values given in Table 1 although the difference is minor. The pore size distribution could also be obtained by using mercury intrusion porosimetery [20,41]. In such a technique, mercury, as a nonwetting fluid on most surfaces, is penetrated into the pores of the GDL by applying pressure. The applied pressure is a function of the pore diameter. Williams et al. [1] used this approach and obtained pore size distributions for E-TEK carbon paper, E-TEK carbon cloth, and SGL carbon paper.

In-Plane Variation of Pore Diameter Distribution. The pore diameter distribution for one GDL and at three random locations on its surface is also studied in this work. Figure 6 shows the pore diameter distribution for three different locations on the untreated thickest GDL (TGP_120). Although the mean pore size calculated for all three cases is about 25 μm, the number of pores detected

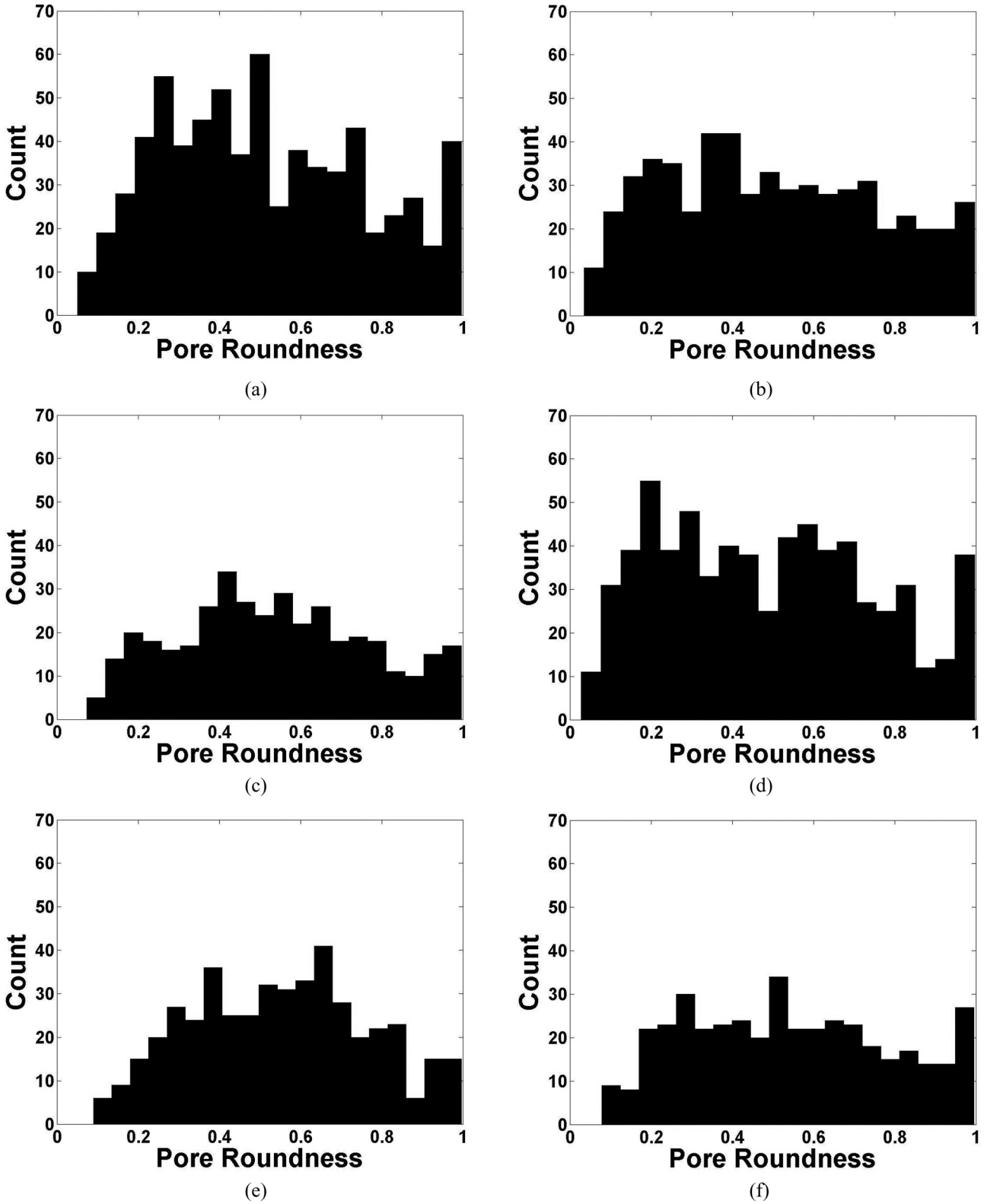

Fig. 7 Pore roundness distribution of GDLs

within each range of diameters are different. Again, it can be observed that the majority of the detected pores have diameters of less than 20 μm, while there are larger pores detected in all three locations.

Pore Roundness Distribution. The pore roundness S is a property that describes the shape of the pores and is defined by Eq. (5)

$$S = 4\pi A/P^2 \tag{5}$$

where A is the pore area and P is the perimeter of the pore. For a perfect circle, the pore roundness is 1 and, as the roundness of the shape decreases, this value also decreases. The pore roundness distributions of GDLs with different thicknesses are given in Fig. 7. In general, no specific trend can be detected based on these

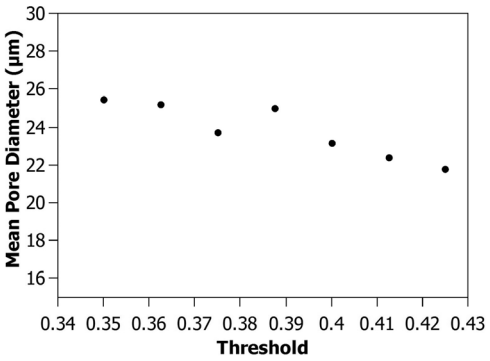

Fig. 8 The variation of the calculated mean pore diameter as a function of the threshold for TGP-060

histograms. It may be concluded that Toray carbon paper pores are mostly in random shapes and do not follow any specific trend of a shape.

Effect of Threshold on Mean Pore Diameter. The MATLAB code processes the SEM images by converting gray level images into binary, based on the Otsu method. The threshold changes the degree of black and white objects in the image and can change the results obtained from the images. In this section, the effect of threshold setting on the mean pore diameter is studied. Figure 8 shows the variation of the mean pore diameter as a function of the threshold for the TGP_060 GDL. The threshold, defined based on the Otsu method, for this image was 0.3875. The MATLAB code was run to obtain the mean pore diameter for different thresholds starting from 0.35 with steps of 0.0125. Figure 8 shows a negligible variation of the mean pore diameter for different threshold settings. This strengthens the validity of the results obtained based on this approach.

Conclusion

The GDL microstructural surface properties for different GDL thicknesses and for the PTFE treated and untreated cases have been studied based on the SEM images obtained. Consequent steps of image processing have been taken and the SEM images were analyzed for the mean pore diameter, pore diameter distribution, and pore roundness as the microstructural properties of the GDL. The droplet static contact angle on the GDLs, as a macroscale surface property, has been measured using a setup made for this purpose. The following conclusions can be drawn from this study:

(1) The GDL thickness was observed to have no effect on the droplet contact angle.
(2) While the droplet contact angles significantly increased from an untreated GDL to a PTFE treated one, the amount of the PTFE content in the GDL was observed to have no impact on the contact angles measured.
(3) The GDL mean pore diameter does not change with its thickness. Furthermore, the mean pore diameter was observed to be the same for untreated and treated GDLs. Using the SEM image, the mean pore diameter was analyzed to be around 26 μm for treated and untreated Toray carbon papers of different thicknesses.
(4) The standard deviation of the mean pore diameter calculated for the untreated GDLs was smaller than for untreated GDLs.
(5) The PTFE loading approach taken in this study resulted in an uneven PTFE distribution on the GDL surface (in-plane).
(6) The threshold value, in the range of the threshold defined by the Otsu method, was observed to have a negligible effect on the mean pore diameter.
(7) The pore diameter distribution plots indicate that the majority of pores fall within less than a 20 μm pore diameter.
(8) The pore roundness distribution plots suggest a nonattributable shape of Toray carbon paper pores.

Acknowledgment

Michigan Technological University is gratefully acknowledged for providing the startup funding for this research. The authors would like to thank Nishith Parikh from the Energy and Nano Science (ENS) Laboratory at Michigan Technological University for taking the SEM images and providing the MATLAB code for the SEM image analysis. Vinaykumar Konduru from the Microfluidic and Interfacial Transport Laboratory at Michigan Technological University is also appreciated for measuring the contact angles of droplets on the GDLs.

References

[1] Williams, M. V., Begg, E., Bonville, L., Kunz, H. R., and Fenton, J. M., 2004, "Characterization of Gas Diffusion Layers for PEMFC," J. Electrochem. Soc., **151**, p. A1173.
[2] Nguyen, T. V., 2006, "Water Management by Material Design and Engineering for PEM Fuel Cells," ECS Trans., **3**, pp. 1171–1180.
[3] Sinha, P. K., Mukherjee, P. P., and Wang, C. Y., 2007, "Impact of GDL Structure and Wettability on Water Management in Polymer Electrolyte Fuel Cells," J. Mater. Chem., **17**(30), pp. 3089–3103.
[4] Bazylak, A., 2009, "Liquid Water Visualization in PEM Fuel Cells: A Review," Int. J. Hydrogen Energy, **34**(9), pp. 3845–3857.
[5] Zhang, F. Y., Yang, X. G., and Wang, C. Y., 2006, "Liquid Water Removal From a Polymer Electrolyte Fuel Cell," J. Electrochem. Soc., **153**, p. A225.
[6] Dai, W., Wang, H., Yuan, Z. Z., Martin, J. J., Yang, D., Qiao, J., and Ma, J., 2009, "A Review on Water Balance in the Membrane Electrode Assembly of Proton Exchange Membrane Fuel Cells," Int. J. Hydrogen Energy, **34**(23), pp. 9461–9478.
[7] Tüber, K., Pócza, D., and Hebling, C., 2003, "Visualization of Water Buildup in the Cathode of a Transparent PEM Fuel Cell," J. Power Sources, **124**(2), pp. 403–414.
[8] Spernjak, D., Prasad, A. K., and Advani, S. G., 2007, "Experimental Investigation of Liquid Water Formation and Transport in a Transparent Single-Serpentine PEM Fuel Cell," J. Power Sources, **170**, pp. 334–344.
[9] Yang, X. G., Zhang, F. Y., Lubawy, A. L., and Wang, C. Y., 2004, "Visualization of Liquid Water Transport in a PEFC," Electrochem. Solid-State Lett., **7**, p. A408.
[10] Theodorakakos, A., Ous, T., Gavaises, M., Nouri, J. M., Nikolopoulos, N., and Yanagihara, H., 2006, "Dynamics of Water Droplets Detached From Porous Surfaces of Relevance to PEM Fuel Cells," J. Colloid Interface Sci., **300**(2), pp. 673–687.
[11] Hickner, M. A., Siegel, N. P., Chen, K. S., Hussey, D. S., Jacobson, D. L., and Arif, M., 2008, "In Situ High-Resolution Neutron Radiography of Cross-Sectional Liquid Water Profiles in Proton Exchange Membrane Fuel Cells," J. Electrochem. Soc., **155**, p. B427.
[12] Niroumand, A. M. and Saif, M., 2010, "Two-Phase Flow Measurement System for Polymer Electrolyte Fuel Cells," J. Power Sources, **195**(10), pp. 3250–3255.
[13] Lin, G. and Nguyen, T. V., 2005, "Effect of Thickness and Hydrophobic Polymer Content of the Gas Diffusion Layer on Electrode Flooding Level in a PEMFC," J. Electrochem. Soc., **152**, pp. A1942–A1948.
[14] Park, G. G., Sohn, Y. J., Yang, T. H., Yoon, Y. G., Lee, W. Y., and Kim, C. S., 2004, "Effect of PTFE Contents in the Gas Diffusion Media on the Performance of PEMFC," J. Power Sources, **131**, pp. 182–187.
[15] Pasaogullari, U. and Wang, C. Y., 2004, "Liquid Water Transport in Gas Diffusion Layer of Polymer Electrolyte Fuel Cells," J. Electrochem. Soc., **151**, p. A399.
[16] Nam, J. H. and Kaviany, M., 2003, "Effective Diffusivity and Water-Saturation Distribution in Single- and Two-Layer PEMFC Diffusion Medium," Int. J. Heat Mass Transfer, **46**(24), pp. 4595–4611.
[17] Litster, S., Sinton, D., and Djilali, N., 2006, "Ex Situ Visualization of Liquid Water Transport in PEM Fuel Cell Gas Diffusion Layers," J. Power Sources, **154**(1), pp. 95–105.
[18] Defay, R. and Prigogine, I., 1966, *Surface Tension and Adsorption*, Wiley, New York.
[19] Tamayol, A. and Bahrami, M., 2011, "Water Permeation Through Gas Diffusion Layers of Proton Exchange Membrane Fuel Cells," J. Power Sources, **196**(15), pp. 6356–6361.
[20] Gostick, J. T., Ioannidis, M. A., Fowler, M. W., and Pritzker, M. D., 2009, "Wettability and Capillary Behavior of Fibrous Gas Diffusion Media for Polymer Electrolyte Membrane Fuel Cells," J. Power Sources, **194**(1), pp. 433–444.
[21] Gostick, J. T., Fowler, M. W., Pritzker, M. D., Ioannidis, M. A., and Behra, L. M., 2006, "In-Plane and Through-Plane Gas Permeability of Carbon Fiber Electrode Backing Layers," J. Power Sources, **162**(1), pp. 228–238.
[22] Hwang, C. M., Ishida, M., Ito, H., Maeda, T., Nakano, A., Hasegawa, Y., Yokoi, N., Kato, A., and Yoshida, T., 2010, "Influence of Properties of Gas Diffusion Layers on the Performance of Polymer Electrolyte-Based Unitized Reversible Fuel Cells," Int. J. Hydrogen Energy, **36**, p. 1740.

[23] MnIT Research Group, 2013, "Microfluidics Laboratory," Michigan Technological University, Houghton, MI, http://www.me.mtu.edu/mnit/
[24] Konduru, V., 2010, "Static and Dynamic Contact Angle Measurement on Rough Surfaces Using Sessile Drop Profile Analysis With Application to Water Management in Low Temperature Fuel Cells," Master's thesis, Michigan Technological University, Houghton, MI.
[25] Parikh, N., Allen, J., and Yassar, R. S., 2012, "Microstructure of Gas Diffusion Layers for PEM Fuel Cells," Fuel Cells, **12**(3), pp. 382–390.
[26] Leinhardt, G. and Leinhardt, S., 1980, "Exploratory Data Analysis: New Tools for the Analysis of Empirical Data," *Review of Research in Education*, Vol. 8, American Educational Research Association, Washington, DC, pp. 85–157.
[27] Sezgin, M. and Sankur, B., 2004, "Survey Over Image Thresholding Techniques and Quantitative Performance Evaluation," J. Electron. Imaging, **13**(1), pp. 146–168.
[28] Otsu, N., 1979, "A Threshold Selection Method From Gray-Level Histograms," IEEE Trans. Systems, Man Cybernetics, **9**(1), pp. 62–66.
[29] Kumbur, E. C., Sharp, K. V., and Mench, M. M., 2006, "Liquid Droplet Behavior and Instability in a Polymer Electrolyte Fuel Cell Flow Channel," J. Power Sources, **161**(1), pp. 333–345.
[30] Whitesides, G. M. and Laibinis, P. E., 1990, "Wet Chemical Approaches to the Characterization of Organic Surfaces: Self-Assembled Monolayers, Wetting, and the Physical-Organic Chemistry of the Solid-Liquid Interface," Langmuir, **6**(1), pp. 87–96.
[31] Fairweather, J. D., Cheung, P., and Schwartz, D. T., 2010, "The Effects of Wetproofing on the Capillary Properties of Proton Exchange Membrane Fuel Cell Gas Diffusion Layers," J. Power Sources, **195**(3), pp. 787–793.
[32] Benziger, J., Nehlsen, J., Blackwell, D., Brennan, T., and Itescu, J., 2005, "Water Flow in the Gas Diffusion Layer of PEM Fuel Cells," J. Membr. Sci., **261**(1–2), pp. 98–106.
[33] Jennings, B. R. and Parslow, K., 1988, "Particle Size Measurement: The Equivalent Spherical Diameter," Proc. Roy. Soc. London, Ser. A, **419**(1856), pp. 137–149.
[34] Dullien, F. A. L., 1992, *Porous Media: Fluid Transport and Pore Structure*, 2nd ed., Academic, New York.
[35] Ihonen, J., Mikkola, M., and Lindbergh, G., 2004, "Flooding of Gas Diffusion Backing in PEFCs, Physical and Electrochemical Characterization," J. Electrochem. Soc., **151**(8), pp. A1152–A1161.
[36] Liu, T. L., and Pan, C., 2012, "Visualization and Back Pressure Analysis of Water Transport Through Gas Diffusion Layers of Proton Exchange Membrane Fuel Cell," J. Power Sources, **207**, pp. 60–69.
[37] Bazylak, A., Sinton, D., and Djilali, N., 2008, "Dynamic Water Transport and Droplet Emergence in PEMFC Gas Diffusion Layers," J. Power Sources, **176**(1), pp. 240–246.
[38] Rofaiel, A., Ellis, J. S., Challa, P. R., and Bazylak, A., 2012, "Heterogeneous Through-Plane Distributions of Polytetrafluoroethylene in Polymer Electrolyte Membrane Fuel Cell Gas Diffusion Layers," J. Power Sources, **201**, pp. 219–225.
[39] Lim, C. and Wang, C. Y., 2004, "Effects of Hydrophobic Polymer Content in GDL on Power Performance of a PEM Fuel Cell," Electrochim. Acta, **49**(24), pp. 4149–4156.
[40] Fishman, Z. and Bazylak, A., 2011, "Heterogeneous Through-Plane Porosity Distributions for Treated PEMFC GDLs: I. PTFE Effect," J. Electrochem. Soc., **158**, p. B841.
[41] Gallagher, K. G., Darling, R. M., Patterson, T. W., and Perry, M. L., 2008, "Capillary Pressure Saturation Relations for PEM Fuel Cell Gas Diffusion Layers," J. Electrochem. Soc., **155**, p. B1225.